Infrared Zeeman study of the Nd^{3+}-Cu^{2+} anisotropic exchange interaction in Nd_2CuO_4

P. Richard*
Département de Physique, Université de Sherbrooke, Sherbrooke, Canada J1K 2R1
and Department of Physics, Boston College, Chestnut Hill, Massachusetts 02134, USA

S. Jandl, M. Poirier, and P. Fournier
Département de Physique, Université de Sherbrooke, Sherbrooke, Canada J1K 2R1

V. Nekvasil
Institute of Physics, Czech Academy of Sciences, Cukrovarnická 10, 162 53 Praha 6, Czech Republic

M. L. Sadowski
Grenoble High Magnetic Field Laboratory, 25 Avenue des Martyrs, B.P. 166 Grenoble, 38042 Grenoble Cédex 09, France
(Received 8 February 2005; published 5 July 2005; publisher error corrected 6 July 2005)

We have performed a Zeeman crystal-field infrared transmission study of Nd_2CuO_4. While a large discrepancy between the Zeeman calculations and the experimental data is observed below a magnetic field of 4 T applied either along the [100] or the [110] directions, the Zeeman calculations are in good agreement with the experimental data above that critical field. This indicates the suppression, above 4 T, of the Nd^{3+}-Cu^{2+} anisotropic exchange interaction responsible for the nonzero Kramers doublet splittings observed in this compound. We show that the noncollinear→collinear transition of the magnetic structure is not responsible for this phenomena. This behavior is explained by a progressive spin reorientation of the Nd^{3+} spins from an antiferromagnetic to a paramagnetic configuration. For $\mathbf{H}\|[001]$, the exchange interaction is not significantly affected. Moreover, it is observed that the Nd^{3+}-Nd^{3+} interactions, which modify only slightly the Kramers doublet splittings, is opposite to both the Nd^{3+}-Cu^{2+} anisotropic exchange and the Zeeman interactions.

DOI: 10.1103/PhysRevB.72.014506 PACS number(s): 74.25.Ha, 71.70.Gm, 71.70.Ej, 74.72.Jt

I. INTRODUCTION

In the study of high-T_c superconductivity, the magnetic properties have been the subject of many investigations. Even though most of these studies concern hole-doped materials, some of them have been devoted to the so-called 2-1-4 electron-doped superconductors ($RE_{2-x}Ce_xCuO_4$, RE =Pr, Nd, Sm). These compounds exhibit several interesting magnetic properties. Among them, their low upper critical field allowed experiments to establish the antiferromagnetic (AF) order as a competing ground state in the electron-doped superconductors.[1] Furthermore, these materials are known to exhibit an AF order for doping as high as the optimal cerium concentration $x=0.15$,[2] in opposition to hole materials for which only a low concentration of charge carriers suppresses the AF order.

Due to the strongly coupled Cu^{2+} and Nd^{3+} magnetic subsystems, Nd_2CuO_4 is certainly the most interesting of these compounds from a magnetic point of view. Its strong magnetic coupling is manifested by spin reorientations found around 33 K and 70 K, well below the Cu^{2+} Néel temperature [~250 K (Refs. 3–6)], using several experimental techniques, such as ultrasonic interferometry,[7] muon spin relaxation,[4] and neutron measurements.[5,8,9] The three corresponding magnetic phases are designed as Phase I ($70\ \mathrm{K} \lesssim T \lesssim 250\ \mathrm{K}$), Phase II ($33\ \mathrm{K} \lesssim T \lesssim 70\ \mathrm{K}$), and Phase III ($T \lesssim 33$ K), respectively. The spin reorientations characterizing the phase transitions are described in terms of three-layer-spin units, formed by one Cu^{2+} layer sandwiched between two Nd^{3+} layers, which rotate as a whole by 90° in the *ab* plane, with the adjacent unit rotating in the opposite direction. Furthermore, the large enhancement of the Nd^{3+} moment at low temperature is responsible for locally distorted magnetic domains below 5 K.[7] The magnetic structure of Nd_2CuO_4 remains noncollinear[10–12] until a magnetic field of 4.4 T and 0.75 T is applied along the [100] and the [110] directions, respectively.[10] These field-induced transitions are accompanied by the closure of a 0.3 meV gap in an acoustic magnon branch at $\mathbf{k}=0$, leading to magnon heat transport at a temperature as high as 18 K.[13]

Although the orientation of the Cu^{2+} spins is quite well known, the Cu^{3+}-Nd^{3+} and the Nd^{3+}-Nd^{3+} interactions are not well understood, the ordering of the Nd^{3+} remaining controversial. While x-ray magnetic scattering data indicate that Nd^{3+} ions are polarized at 37 K,[14] an enhancement of neutron scattering magnetic peak intensities around 3 K has been interpreted by Matsuda *et al.* as evidence for a direct Nd^{3+}-Nd^{3+} interaction,[5] whereas Lynn *et al.* have estimated the Nd^{3+} ordering temperature around 1.5 K.[6] Also, a recent ultrasonic investigation of Nd_2CuO_4 has suggested frustrated magnetic structure due to a competition between the Nd^{3+}-Cu^{2+} and the Nd^{3+}-Nd^{3+} interactions at low temperature, which leads to the development of distorted magnetic domains stabilized under magnetic field.[7]

Optical spectroscopy is an appropriate tool to the investigation of magnetic interactions at a microscopic level. Hence, the rare earth crystal-field (CF) energy levels measured by both Raman scattering and infrared transmission give precious information about the rare earths local environment. This is particularly relevant in the case of Nd_2CuO_4,

which possesses Nd^{3+} Kramers ions located in the vicinity of the CuO_2 planes. Owing to time-reversal symmetry, each Nd^{3+} $4f$ crystal-field level has a twofold degeneracy that can be removed only in the presence of either an external magnetic field or an exchange interaction. The Nd^{3+} Kramers doublet (KD) splittings in zero applied magnetic field have allowed the characterization of the Cu^{2+} spin reorientations in Nd_2CuO_4 by both Raman scattering[15] and infrared transmission spectroscopy.[16] These splittings are observed using infrared transmission at a temperature as high as 140 K, indicating that the Nd^{3+} spins are already polarized at these temperatures, in Phase I.[16] The Nd^{3+}-Cu^{2+} exchange interaction responsible for this degeneracy removal has been found to be anisotropic.[17] However, a precise description of this interaction needs further investigations.

To the authors' knowledge, only one Zeeman CF study of Nd_2CuO_4 has been performed, using Raman scattering.[18] In order to avoid complications arising from the Cu^{2+} field-induced spin-flop, only results for magnetic fields higher than 4 T have been examined in detail. In this present paper, we present the first crystal-field infrared transmission study of Nd_2CuO_4 under magnetic field in order (i) to validate the crystal-field parameters obtained in Ref. 19, (ii) to further characterize, below and above 4 T, the anisotropy of the Nd^{3+}-Cu^{2+} exchange interaction from a local point of view and (iii) to investigate the influence of the Nd^{3+}-Nd^{3+} interaction on the low temperature Nd^{3+} KD splittings.

II. EXPERIMENT

Nd_2CuO_4 single crystals have been studied by CF infrared transmission. Measurements have been performed both at the Université de Sherbrooke and at the Grenoble High Magnetic Field Laboratory. The Sherbrooke setup, adapted for measurements under magnetic field (0 T–7.5 T), consists of a Michelson interferometer (Bomem DA3.002) equipped with an InSb detector, a CaF_2 beam splitter and both globar and quartz sources. This allowed us to record 1 cm^{-1} resolution spectra, between 8 and 50 K, in the 1800–7000 cm^{-1} spectral range. In the Grenoble setup, the sample was placed in the bore of a superconducting magnet, in a helium bath cryostat at 1.6 K. A composite Si bolometer placed directly beneath the sample was used to measure the intensity of the transmitted light. A Bruker Instruments model 113 Fourier Transform Spectrometer, equipped with tungsten and globar light sources, was used to collect and analyze spectra with a resolution of 1 cm^{-1} in the 0 T–13 T magnetic field range.

In order to explore the influence of the magnetic field orientation, three Nd_2CuO_4 single crystals, grown by the flux method,[20] were measured. Sample 1, sample 2, and sample 3 were mounted with the magnetic field aligned along the [100], [110], and [001] directions, respectively, with the unpolarized light beam parallel to the magnetic field. The thickness of the samples in the transmission direction varied between 50 and 80 μm.

III. GROUP ANALYSIS AND NOTATION

Inside a crystal, the free ion energy multiplets $^{2S+1}L_J$ of an ion are split due to the crystal-field Hamiltonian H_{CF} described by Eq. (1),[21]

$$H_{CF} = \sum_{k,q} B_{k,q}(C_q^{(k)} + C_{-q}^{(k)}). \quad (1)$$

In this equation, the $(2k+1)$ operators $C_q^{(k)}$ $(q=k,k-1,\ldots,-k)$ are the components of a rank k irreducible tensor and the B_{kq} coefficients represent the CF parameters specific to each local environment. The energy levels resulting from the C_{4v} symmetry site of Nd^{3+} in Nd_2CuO_4, in the absence of an external magnetic field, as well as the corresponding selection rules, are well known.[19] Owing to the Kramers nature of the Nd^{3+} ions, all these levels are twofold-degenerate and transform either as the Γ_6 or the Γ_7 irreducible representations of the C_{4v}^* double group. Particularly, the ground state Kramers doublet (GSKD) of the Nd^{3+} ion in Nd_2CuO_4 has a Γ_6 symmetry, and each transition observed at low temperature are either of the $\Gamma_6 \rightarrow \Gamma_6$ or the $\Gamma_6 \rightarrow \Gamma_7$ types.[19] The CF absorption bands corresponding to the latter case have been found experimentally to be weaker than the CF excitations associated with the $\Gamma_6 \rightarrow \Gamma_6$ transitions.[19]

Under an external applied magnetic field **H**, the KDs split according to the Zeeman Hamiltonian,

$$H_{Zeeman} = -\mu_B(\mathbf{L} + g_s\mathbf{S}) \cdot \mathbf{H}, \quad (2)$$

where **S** and **L** are the total spin and orbital moments, while μ_B and g_s correspond to the Bohr magneton and the spin gyromagnetic factor, respectively.

The lowering symmetry of the Nd^{3+} ion point group in Nd_2CuO_4 depends on the external magnetic field orientation. For $\mathbf{H}\|\hat{\mathbf{z}}$, the symmetry is lowered to C_4 and the two-dimensional Γ_6 and Γ_7 irreducible representations of the C_{4v}^* double group are decomposed, within the C_4^* double group, into $\Gamma_5 \oplus \Gamma_6$ and $\Gamma_7 \oplus \Gamma_8$ one-dimensional irreducible representation sums, respectively.[22] The relevant direct products within the C_4^* double group are given in Ref. 22. According to these products, a C_{4v}^* $\Gamma_6 \rightarrow \Gamma_6$ CF transition of Nd^{3+} in Nd_2CuO_4 splits, under $\mathbf{H}\|\hat{\mathbf{z}}$, into four C_4^* transitions which are all infrared active, two of them ($\Gamma_5 \rightarrow \Gamma_6$ and $\Gamma_6 \rightarrow \Gamma_5$) being not active within our optical configuration (the unpolarized incident beam being perpendicular to the xy plane). Similarly, a C_{4v}^* $\Gamma_6 \rightarrow \Gamma_7$ CF transition of Nd^{3+} in Nd_2CuO_4 splits, under $\mathbf{H}\|\hat{\mathbf{z}}$, into four C_4^* transitions, and only two of them are infrared active ($\Gamma_5 \rightarrow \Gamma_7$ and $\Gamma_6 \rightarrow \Gamma_8$).

For $\mathbf{H}\|\hat{\mathbf{x}}$, the point group symmetry of the Nd^{3+} ion in Nd_2CuO_4 is lowered to C_s and both the two-dimensional Γ_6 and Γ_7 irreducible representations of the C_{4v}^* double group are decomposed, within the C_s^* double group, into the $\Gamma_3 \oplus \Gamma_4$ irreducible representation sum.[22] The relevant C_s^* direct products are given in Ref. 22 [note that x is the principal axis under a magnetic field applied along [100] and we use the (x,y,z) coordinate system of the C_{4v}^* double group to express the appropriate C_s^* basis functions]. In the optical configuration where the sample is mounted with the unpolarized incident beam and the external magnetic field along [100], we expect to observe only two of the four possible transitions between two Nd^{3+} KD ($\Gamma_3 \rightarrow \Gamma_4$ and $\Gamma_4 \rightarrow \Gamma_3$).

The selection rules involved in the configuration for which the magnetic field is applied along the [110] direction (x') and the unpolarized light is perpendicular to the zy'

TABLE I. Crystal-field parameters B_{kq} and bary-center $F(J)$ energies associated with the ^4I_J multiplets used in the Zeeman calculations.

Parameter	Energy (cm^{-1})
B_{20}	−312
B_{40}	−2246
B_{44}	1609
B_{60}	215
B_{64}	1495
$F(9/2)$	296
$F(11/2)$	2155
$F(13/2)$	4115
$F(15/2)$	6141

plane, where $y'=[1\bar{1}0]$, are similar to the previous case. The point group symmetry of the Nd^{3+} ion in Nd_2CuO_4 is also lowered to C_s, with x' as the principal axis. The relevant direct products are the same, with x and y being replaced by x' and y', respectively. As for the previous case, we expect to observe only two of the four possible transitions between two Nd^{3+} KD ($\Gamma_3 \rightarrow \Gamma_4$ and $\Gamma_4 \rightarrow \Gamma_3$).

In order to identify the experimental transitions and splittings, as well as to extract information about the Nd^{3+}-Cu^{2+} exchange interaction, Zeeman calculations of the Nd^{3+} energy levels in Nd_2CuO_4 have been performed for various magnetic field orientations by diagonalizing simultaneously, in the subspace of all four ^4I_J multiplets, H_0 (free-ion Hamiltonian), H_{CF}, and H_{Zeeman}. The discrepancies between the experimental data and the Zeeman calculations are supposed to be due to the Nd^{3+}-Cu^{2+} exchange interaction. The CF parameters used in these calculations, which are refined parameters of Ref. 19, are given in Table I. Multiple electron effects are taken into account by approximating H_0 with the bary-center $F(J)$ of each Nd^{3+} ^4I_J multiplet. These bary-center energies are also given in Table I.

For low temperature spectra, each Nd^{3+} CF excitation corresponds to a transition from the GSKD to an excited KD. Each of these KDs has two components, the lower energy level, called 1, and the higher energy one, called 2. Hence, neglecting the previously mentioned selection rules, there are four possible transitions involving two KDs. To simplify, we have introduced the following notation: we call $\langle i \rightarrow j:D \rangle$, where i and j can be 1 or 2, the transition from the ith energy level of the GSKD to the jth energy level of the excited KD of D energy (in cm^{-1}) as reported in Ref. 19.

For the sake of clarity, we now detail the convention used in the figures and in the text. Each Nd^{3+} regular site CF transition observed in the Nd_2CuO_4 spectra (Figs. 1, 3, and 5) that has been assigned using the Zeeman calculations, is labeled with an italic symbol, while the Nd^{3+} regular site CF transitions that could not be assigned to a specific transition, due to band overlapping, band broadness or saturation, are labeled with greek symbols. The transitions related to a Nd^{3+} ion in the vicinity of an apical oxygen[23] are identified with asterisks. The positions of the assigned Nd^{3+} regular site CF excitations as a function of the external magnetic field are reported with the Zeeman calculations (Figs. 2, 4, and 6). In these figures, open circles and squares are associated, respectively, with $\langle 1 \rightarrow j:D \rangle$ and $\langle 2 \rightarrow j:D \rangle$ transitions observed at 8.5 K, while open upward and downward triangles correspond to $\langle 1 \rightarrow j:D \rangle$ and $\langle 2 \rightarrow j:D \rangle$ transitions observed at 1.6 K, respectively. The black squares are associated with assigned $\langle 2 \rightarrow j:D \rangle$ transitions detected at 40 K. On the other hand, each calculated $\langle 1 \rightarrow j:D \rangle$ transition is represented by a solid line while the dashed lines correspond to $\langle 2 \rightarrow j:D \rangle$ transitions.

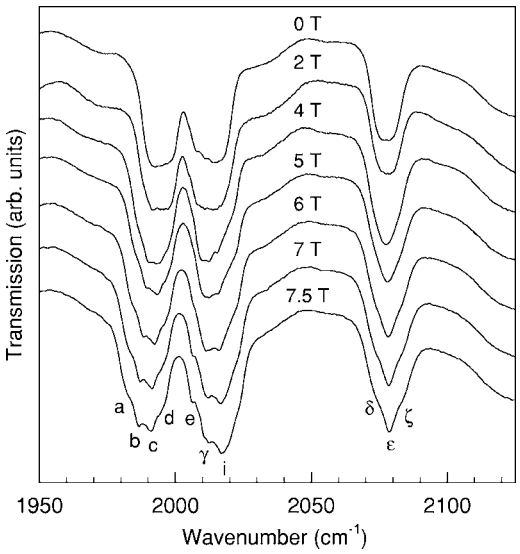

FIG. 1. Nd^{3+} $^4I_{9/2} \rightarrow {}^4I_{11/2}$ low temperature spectra (8.5 K) of sample 1 for $\mathbf{H} \| [001]$. Italic and greek symbols correspond to assigned and unassigned Nd^{3+} regular site CF excitations, respectively.

IV. RESULTS

A. H‖[001]

As suggested by the strongly anisotropic magnetic susceptibility of Nd_2CuO_4,[24] which is governed by the Nd^{3+} magnetic moments, the GSKD splitting is expected to be small for a field applied along [001]. The experimental spectra corresponding to that configuration are reported in Fig. 1. In that configuration, CF excitations associated with the Nd^{3+} ion in a regular site have been detected only in the 1950–2100 cm^{-1} spectral range, which corresponds to transitions from the GSKD to the Nd^{3+} $^4I_{11/2}$ multiplet. While four of them could not be associated with precise transitions (γ, δ, ϵ, and ζ), six CF excitations have been assigned to precise transitions (a, b, c, d, e, and i).

In order to assign these transitions, their energies have been plotted in Fig. 2 as a function of the applied magnetic field, and compared with Zeeman calculations. The transitions labeled a, b, c, and d have been associated with the $\langle 2 \rightarrow 1:1995 \rangle$, $\langle 1 \rightarrow 1:1995 \rangle$, $\langle 2 \rightarrow 2:1995 \rangle$, and $\langle 1 \rightarrow 2:1995 \rangle$ transitions, respectively. The associated splittings, already nonzero in the absence of a magnetic field, increase slightly. Hence, the splitting d-a is enhanced from

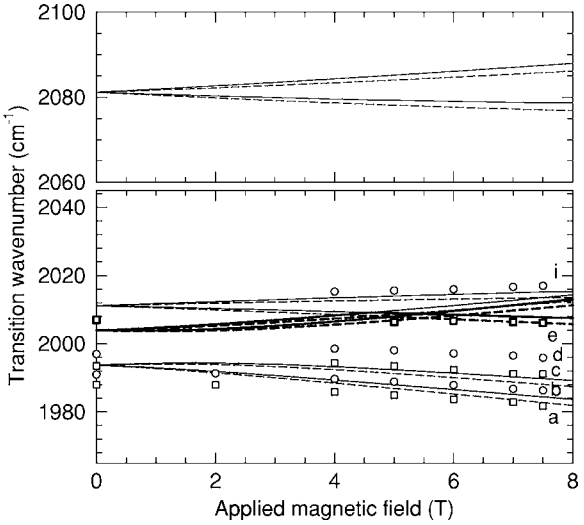

FIG. 2. Comparison between the Zeeman calculations and the experimental data in the Nd^{3+} $^4I_{9/2} \rightarrow {}^4I_{11/2}$ spectral range for $\mathbf{H} \| [001]$. Solid and dashed lines correspond to calculated transitions from the lowest and highest energy component of the GSKD, respectively. Circles and squares are associated with assigned Nd^{3+} regular site experimental transitions at 8.5 K starting from the lowest and the highest energy component of the GSKD, respectively.

9 to 14 cm^{-1} as the applied magnetic field reaches 7.5 T. The situation is less clear around 2010 cm^{-1}, where two KDs overlap. This is why only two CF excitations, *e* and *i*, have been assigned. They are associated with the $\langle 2 \rightarrow 1 : 2006 \rangle$ and $\langle 1 \rightarrow 2 : 2013 \rangle$ transitions, respectively.

Even though some transitions could not be assigned, one can conclude that the Nd^{3+}-Cu^{2+} contribution to the KD splittings remain almost unchanged as a magnetic field ($\leqslant$7.5 T) is applied along the *z* axis. The discrepancy between the observed *d*-*a* splitting and the corresponding Zeeman calculations varies only from 9 to 7 cm^{-1} as the maximum magnetic field is reached. This indicates that the Nd^{3+}-Cu^{2+} exchange interaction is not significantly modified. The small variations are associated with a canting of the Nd^{3+} spins out of the *xy* plane, as observed in an ultrasonic study of Nd_2CuO_4.[7]

B. H ⊥ [001]

The influence of a magnetic field on the Nd^{3+} KDs is expected to be more important for a magnetic field applied perpendicularly to [001]. It is of interest to measure the Nd^{3+} KD splittings for a magnetic field applied both along the [100] and the [110] directions, in order to investigate the possible consequences of the field-induced spin reorientations on the Nd^{3+}-Cu^{2+} exchange interaction.

Figures 3(a) and 3(b) show the experimental spectra related to transitions from the GSKD to the $^4I_{11/2}$ multiplet, for a magnetic field applied along [100] and [110], respectively. Many transitions corresponding to regular site Nd^{3+} CF excitations are observed. As for the $\mathbf{H} \|$ [001] configuration, Zeeman calculations have been performed for a magnetic field applied along the [100] and [110] directions.

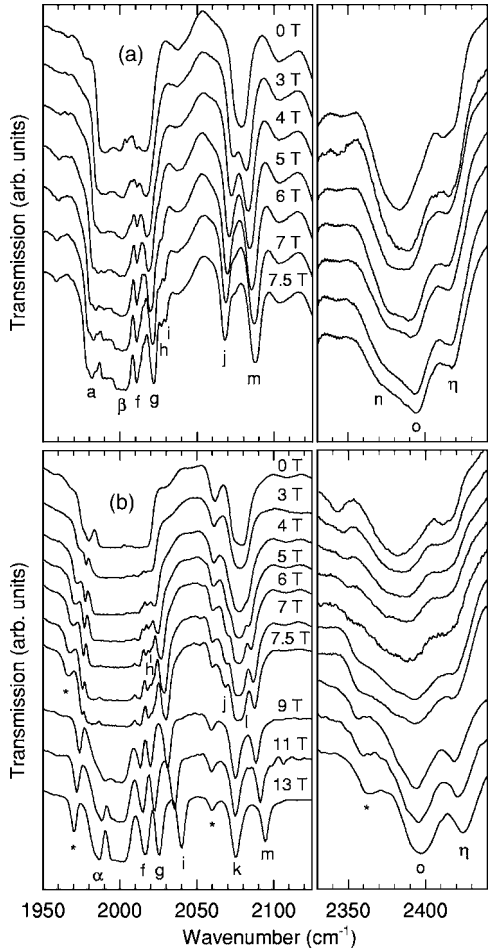

FIG. 3. Nd^{3+} $^4I_{9/2} \rightarrow {}^4I_{11/2}$ low temperature spectra of (a) sample 2 for $\mathbf{H} \| [100]$; (b) sample 3 for $\mathbf{H} \| [110]$. Each spectrum with $\mathbf{H} < 8$ T and $\mathbf{H} > 8$ T has been obtained at 8.5 and 1.6 K, respectively. Italic and greek symbols correspond to assigned and unassigned Nd^{3+} regular site CF excitations, respectively, while asterisks are associated with CF transitions of Nd^{3+} in the vicinity of an apical oxygen.

The calculations for $\mathbf{H} \| [100]$ and [110] corresponding to the GSKD $\rightarrow {}^4I_{11/2}$ spectral range are shown in Figs. 4(a) and 4(b), respectively. In both cases, the 1995, 2006, and 2013 cm^{-1} KDs overlap significantly. This complicates significantly the identification of the transitions. Moreover, this spectral region is characterized by a saturated absorption band around 1995 cm^{-1}, which prevents accurate identification of the possible transitions. For these reasons, two regular site Nd^{3+} CF excitations have not been assigned in both $\mathbf{H} \| [100]$ (β and η) and $\mathbf{H} \| [110]$ (α and η) cases. Another source of complication for sample 3 spectra, obtained under a magnetic field applied along [110], is the presence of apical oxygens, as shown by the transitions identified with asterisks. A previous infrared study of Nd_2CuO_4 has associated these transitions with Nd^{3+} ions in the vicinity of apical oxygens.[23] Three of them are detected in this spectral region, around 1975, 2061, and 2364 cm^{-1} in absence of magnetic field.

Despite these complications, nine GSKD $\rightarrow {}^4I_{11/2}$ experimental CF excitations (*a*, *f*, *g*, *h*, *i*, *j*, *m*, *n*, and *o*) have been

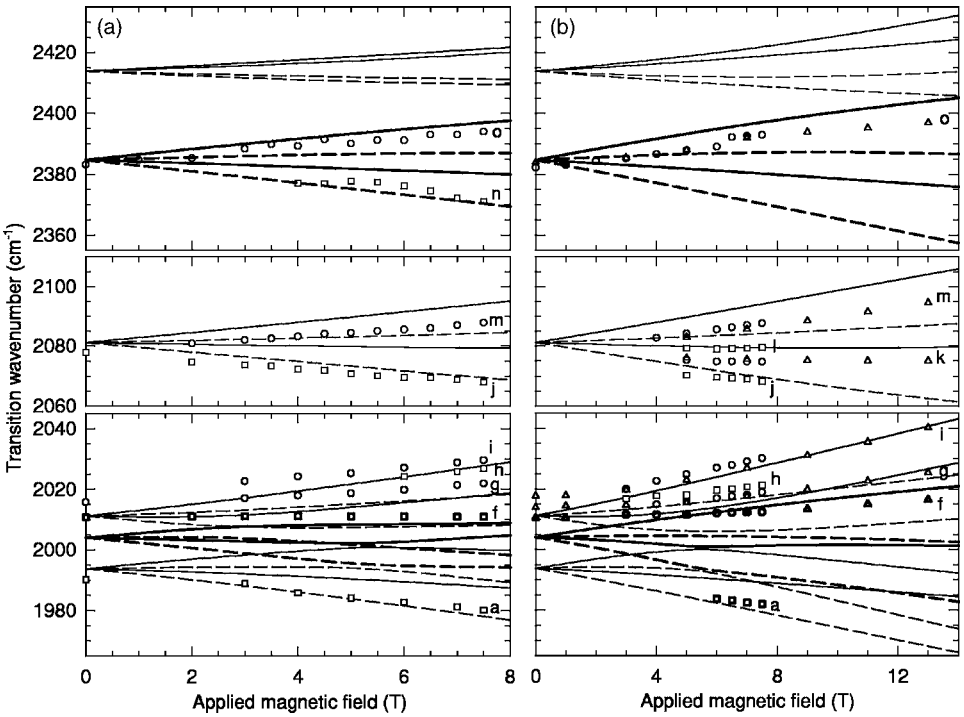

FIG. 4. Comparison between the Zeeman calculations and the experimental data in the Nd^{3+} $^4I_{9/2} \rightarrow {}^4I_{11/2}$ spectral range for (a) $\mathbf{H}\|[100]$ or (b) $\mathbf{H}\|[110]$. Solid and dashed lines correspond to calculated transitions from the lowest and highest energy component of the GSKD, respectively. Circles (upward triangles) and squares (downward triangles) are associated with Nd^{3+} regular site assigned experimental transitions at 8.5 K (1.6 K) starting from the lowest and the highest energy component of the GSKD, respectively.

tentatively assigned for a field applied along [100], while 10 transitions (*a*, *f*, *g*, *h*, *i*, *j*, *k*, *l*, *m*, and *o*) have been assigned for $\mathbf{H}\|[110]$. The CF excitation labeled *a*, which corresponds to the $\langle 2 \rightarrow 1:1995 \rangle$ transition, is observed at 8.5 K for each field orientation, in good agreement with the calculations, but is not resolved at 1.6 K. The *f* transition, assigned to the $\langle 1 \rightarrow 2:2006 \rangle$ transition, is well resolved for both field orientations, as well as at 1.6 and 8.5 K. The *g*, *h*, and *i* CF excitations are associated, respectively, to the $\langle 1 \rightarrow 1:2013 \rangle$, $\langle 2 \rightarrow 2:2013 \rangle$, and $\langle 2 \rightarrow 1:2013 \rangle$ transitions. In contrast to the *g* and *i* transitions, observed for each field orientation and at 1.6 and 8.5 K, the *h* transition is not observed at 1.6 K. The Zeeman calculations do not fit very well the experimental data for the *g*, *h*, and *i* CF excitations, due to the level mixing. Assuming a constant shift of the corresponding calculated transitions, the fits are better for the 2077 cm^{-1} KD, since that one is isolated. While only the *j* and *m* CF excitations are observed for $\mathbf{H}\|[100]$, all the possible *j*, *k*, *l*, and *m* transitions, which correspond, respectively, to the $\langle 2 \rightarrow 1:2077 \rangle$, $\langle 1 \rightarrow 1:2077 \rangle$, $\langle 2 \rightarrow 2:2077 \rangle$, and $\langle 1 \rightarrow 2:2077 \rangle$ transitions, are detected for $\mathbf{H}\|[110]$. However, the uncertainty on the energy levels is not negligible, due to band overlapping. Contrary to the *j* and *l* transitions, the *m* and *k* transitions are still observed at 1.6 K, confirming that they involve the lowest energy level of the GSKD. The broad bands between 2350 and 2440 cm^{-1} are associated with the 2383 and 2484 cm^{-1} KDs. For $\mathbf{H}\|[100]$, the *n* and *o* CF excitations are observed and assigned to the $\langle 2 \rightarrow 1:2383 \rangle$ and $\langle 1 \rightarrow 2:2383 \rangle$ transitions, respectively. The *n* transition is not resolved for $\mathbf{H}\|[110]$.

It is noteworthy that the data corresponding to the Nd^{3+} GSKD $\rightarrow {}^4I_{11/2}$ spectral range indicate a small modification in the KD splittings obtained at 1.6 K and 8.5 K. While no significant shift in temperature is observed for the *f* and *g* transitions, a non-negligible shift is observed for the *i*, *k*, and *m* CF excitations. The decrease of the KD splittings imply a decrease of the $\langle 1 \rightarrow 2:D \rangle$ transition energies and an increase of the $\langle 2 \rightarrow 1:D \rangle$ ones. Similarly, a shift towards the low (high) and the high (low) energies is expected, respectively, for $\langle 1 \rightarrow 1:D \rangle$ and $\langle 2 \rightarrow 2:D \rangle$ transitions if the *D* KD splitting is smaller (larger) than GSKD's. The *i* and the *m* CF excitations, both associated with $\langle 1 \rightarrow 2:D \rangle$ transitions, have decreasing energies with a decrease of the temperature from 8.5 K to 1.6 K, while the energy of the *k* CF excitation, assigned to the $\langle 1 \rightarrow 1:2077 \rangle$ transition with the 2077 cm^{-1} KD splitting being larger than the GSKD one, is higher at 1.6 K. These three transitions suggest that the splittings at 1.6 K are smaller than those at 8.5 K. Nevertheless, the differences are only around 1 cm^{-1} at 7 T.

Similarly to the previous spectral range, Nd^{3+} GSKD $\rightarrow {}^4I_{13/2}$ spectra, not shown in this paper, exhibit KD overlaps and saturating absorption bands. The last spectral range shown in this paper corresponds to the Nd^{3+} GSKD $\rightarrow {}^4I_{15/2}$ CF excitations. In contrast to the Nd^{3+} $^4I_{11/2}$ and the Nd^{3+} $^4I_{13/2}$ multiplets, the KDs of the Nd^{3+} $^4I_{15/2}$ multiplet do not overlap. The corresponding low temperature spectra (8.5 K) for $\mathbf{H}\|[100]$ and $\mathbf{H}\|[110]$ are given in Figs. 5(a) and 5(b), respectively. Contrary to the $^4I_{11/2}$ and $^4I_{13/2}$ spectral regions, no absorption band saturates. Hence, only two Nd^{3+} regular site CF excitations have not been assigned for $\mathbf{H}\|[100]$ (θ and κ). Furthermore, the spectra performed at 40 K indicate that the unassigned θ absorption band splits into two more assigned CF excitations, *t* and *u*, as shown in the inset of Fig. 5(a), which compares the 5845–5900 cm^{-1} range spectra obtained at 8.5 and 40 K under a magnetic field of 7.5 T applied along [100]. The sample 3 spectra show again CF excitations related to Nd^{3+} ions in the vicinity of apical oxygens, around 5898, 6380, and 6549 cm^{-1}. Figures 6(a) and 6(b) give the energy of the assigned regular site

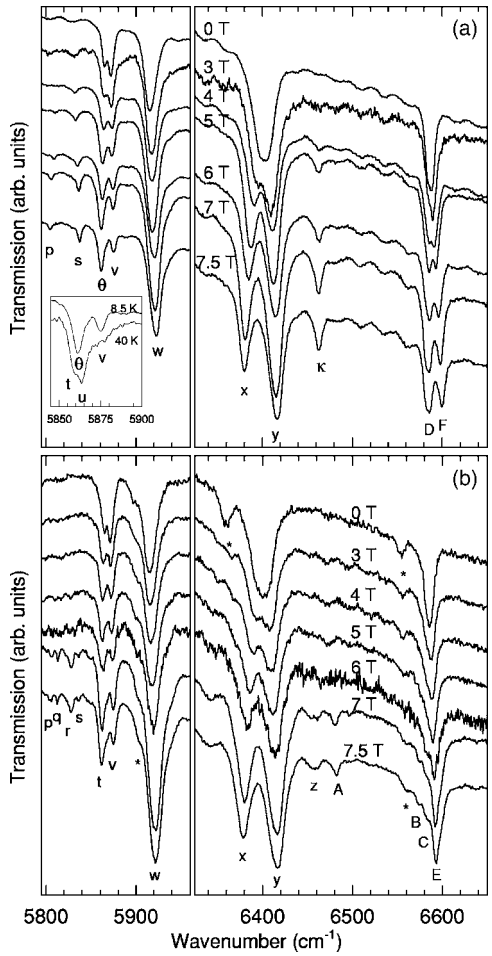

FIG. 5. Nd^{3+} $^4I_{9/2} \rightarrow {}^4I_{15/2}$ low temperature spectra (8.5 K) of (a) sample 2 for $\mathbf{H} \| [100]$; (b) sample 3 for $\mathbf{H} \| [110]$. Italic and greek symbols correspond to assigned and unassigned Nd^{3+} regular site CF excitations, respectively, while asterisks are associated with CF transitions of Nd^{3+} in the vicinity of an apical oxygen. The inset of (a) compares the 5845–5900 cm^{-1} spectral range of the spectra recorded at 8.5 and 40 K under 7.5 T.

Nd^{3+} CF excitations as a function of magnetic field applied along the [100] and [110] directions, respectively, as well as the corresponding Zeeman calculations.

Eight and 14 regular site Nd^{3+} CF excitations have been assigned, respectively, for $\mathbf{H} \| [100]$ (*p*, *s*, *v*, *w*, *x*, *y*, *D*, and *F*) and $\mathbf{H} \| [110]$ (*p*, *q*, *r*, *s*, *t*, *v*, *w*, *x*, *y*, *z*, *A*, *B*, *C*, and *E*). The *p*, *q*, *r*, and *s* CF excitations, which are not observed at low field, are associated with the $\langle 2 \rightarrow 1:5824 \rangle$, $\langle 1 \rightarrow 1:5824 \rangle$, $\langle 2 \rightarrow 2:5824 \rangle$, and $\langle 1 \rightarrow 2:5824 \rangle$ transitions, respectively. While all these CF excitations are detected for $\mathbf{H} \| [110]$, only the *p* and *s* transitions are detected with the field applied along [100]. Assuming a constant shift of the energies, these experimental CF excitations are in good agreement with the Zeeman calculations. The 5868 cm^{-1} KD is involved in the *t*, *u*, and *v* CF excitations, which are associated with the $\langle 2 \rightarrow 1:5868 \rangle$, $\langle 2 \rightarrow 2:5868 \rangle$, and $\langle 1 \rightarrow 2:5868 \rangle$ transitions, respectively. While these three CF excitations have been observed for $\mathbf{H} \| [100]$, only the *t* and *v* CF excitations have been detected for $\mathbf{H} \| [100]$. For both magnetic field configurations, the experimental data are well fitted by the Zeeman calculations above 4 T. A significant discrepancy is observed below that field.

The *w* CF excitation, which is detected in the two magnetic field configurations, is assigned to the $\langle 1 \rightarrow 1:5914 \rangle$ transition. The largest Zeeman splitting in the Nd^{3+} GSKD $\rightarrow {}^4I_{15/2}$ spectral range is that of the *x* and *y* CF excitations, which correspond, respectively, to the $\langle 2 \rightarrow 1:6400 \rangle$ and the $\langle 1 \rightarrow 2:6400 \rangle$ transitions. This splitting, observed for $\mathbf{H} \| [100]$ as well as for $\mathbf{H} \| [110]$, is around 38 cm^{-1} at 7.5 K. After a small shift towards higher energies, the Zeeman calculations are in good agreement with the experimental data for a field above 4 T, while a non-negligiable discrepancy is found below 4 T. Weak absorption bands are related to the 6460 cm^{-1} KD, which has never been observed in the absence of an external magnetic field. As shown in Fig. 5, these features increase with the magnetic field strength. For $\mathbf{H} \| [110]$, two CF excitations, *z* and *A*, are tentatively assigned to the $\langle 1 \rightarrow 1:6460 \rangle$ and $\langle 1 \rightarrow 2:6460 \rangle$ transitions, respectively. While no CF excitation related to the 6570 cm^{-1} KD has been resolved with a magnetic field applied along [100], the *B* and *C* CF excitations, associated with the $\langle 2 \rightarrow 2:6570 \rangle$ and $\langle 1 \rightarrow 2:6570 \rangle$ transitions, respectively, have been detected under a magnetic field higher than 6 T applied along the [110] direction. Finally, Fig. 5(a) exhibits the well resolved *D* and *F* CF excitations with $\mathbf{H} \| [100]$, respectively, assigned to the $\langle 2 \rightarrow 1:6585 \rangle$ and the $\langle 1 \rightarrow 2:6585 \rangle$ transitions. While these two transitions are not observed with $\mathbf{H} \| [110]$, another CF excitation, *E*, is associated with the $\langle 1 \rightarrow 1:6585 \rangle$ transition. Each of the *D*, *E*, and *F* CF excitations are in very good agreement with the Zeeman calculations for $\mathbf{H} > 4$ T, while non-negligible discrepancies are observed below 4 T.

To summarize this section, many CF excitations observed under $\mathbf{H} \| [100]$ and $\mathbf{H} \| [110]$ and corresponding to Nd^{3+} KD splittings have been identified with a very good agreement with the Zeeman calculations for $\mathbf{H} > 4$ T. Below that field, many discrepancies are observed. Furthermore, some Nd^{3+} CF excitations have been detected only with a particular magnetic field orientation. This indicates that selection rules are involved. The experimental data also suggest that these selection rules depend on the magnetic field strength. Finally, the Nd^{3+} KD splittings are not significantly modified at 1.6 K as compared to the splittings measured at 8.5 K.

V. DISCUSSION

Even though this section is mostly devoted to the Nd^{3+}-Cu^{2+} anisotropic exchange interaction, we first discuss further the symmetry of the energy levels and the corresponding selection rules. We focus on the anisotropy of the Nd^{3+}-Cu^{2+} exchange interaction itself, which is influenced differently under a magnetic field parallel or perpendicular to [001]. The origin of this interaction, as well as the impact of the Nd^{3+}-Nd^{3+} interaction on the KD splittings at low temperature, is also discussed.

In contrast to the theoretical predictions, some excited KDs are involved in more than two observed CF excitations.

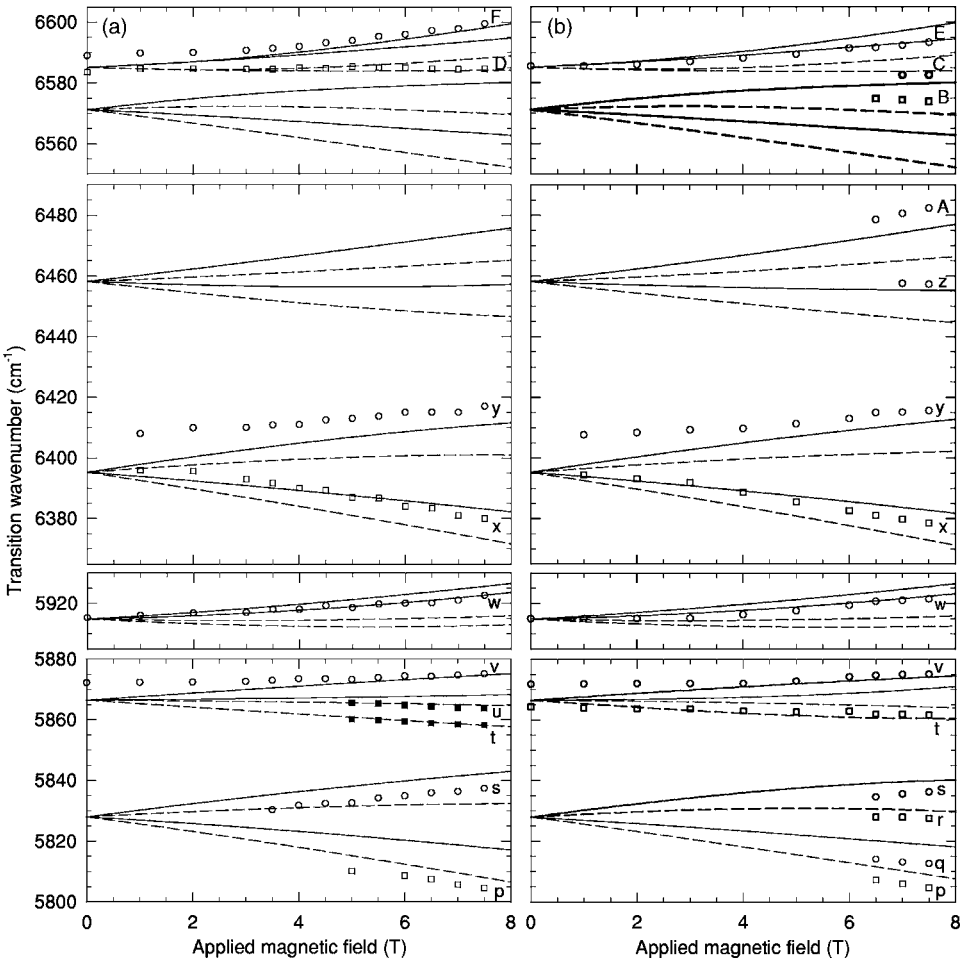

FIG. 6. Comparison between the Zeeman calculations and the experimental data in the Nd^{3+} $^4I_{9/2} \rightarrow {}^4I_{15/2}$ spectral range for (a) $\mathbf{H} \| [100]$ and (b) $\mathbf{H} \| [110]$. Solid and dashed lines correspond to calculated transitions from the lowest and highest energy component of the GSKD, respectively. Circles and white squares are associated with Nd^{3+} regular site assigned experimental transitions at 8.5 K starting from the lowest and the highest energy component of the GSKD, respectively. Black squares refer to assigned transitions detected at 40 K.

Some explanations are considered. First, the exchange interaction can lower the point group symmetry of the Nd^{3+} ions to C_1. In that case, every CF excitation would be theoretically observable. This could explain why four and three low temperature transitions involving, respectively, the 1995 and the 2077 cm^{-1} KD, are observed when the field is applied along [001]. Nevertheless, it cannot explain the data for $\mathbf{H} \perp [001]$ since in that case the exchange interaction vanishes above a critical field, as explained below. Another possibility is the mixing of the closely overlapping energy levels. While this is not confirmed for $\mathbf{H} \| [110]$, most of the well isolated KDs (2077, 2383, 5824, 6400, and 6585 cm^{-1}) are involved, under $\mathbf{H} \| [100]$, in the only two $\langle 2 \rightarrow 1 : D \rangle$ and $\langle 1 \rightarrow 2 : D \rangle$ transitions. The remaining hypotheses to explain the experimental data are a small misalignment of the applied magnetic field with respect to the [100] and [110] directions, that would lower the point group symmetry of the Nd^{3+} ions to C_1, and depolarization effects, that have already been observed in a previous infrared transmission study of Nd_2CuO_4.[16] The depolarization effects would necessarily depend on the light polarization with respect to the crystal axes.

Despite the unknown origin of the selection rules breakdown, the fact that many isolated KDs are involved, under a magnetic field applied along [100], only in the $\langle 2 \rightarrow 1 : D \rangle$ and $\langle 1 \rightarrow 2 : D \rangle$ transitions, suggests that these transitions correspond to C_s^* $\Gamma_3 \rightarrow \Gamma_4$ and $\Gamma_4 \rightarrow \Gamma_3$. This indicates that all KDs, within the C_s^* double group, have their lower (and higher) energy components of the same symmetry. It is also noteworthy that the symmetry lowering due to an external magnetic field is gradual. Even though they split, the KDs maintain residual characters of their C_{4v}^* Γ_6 or Γ_7 symmetry at low field. Consequently, some transitions associated with unfavorable C_{4v}^* $\Gamma_6 \rightarrow \Gamma_7$ are much stronger at high magnetic field.[19] Such behavior is observed in the GSKD $\rightarrow {}^4I_{15/2}$ spectral range, shown in Fig. 5. The p, q, r, and s CF excitations, associated with the 5824 cm^{-1} KD, the z, A, and κ transitions, which are related to the 6460 cm^{-1} KD, as well as the B and C CF excitations, associated with the 6570 cm^{-1} KD, have intensities that become important only under magnetic field. They all involve excited KDs with $C_{4v}^* \Gamma_7$ symmetry in zero field.

We now discuss the Nd^{3+}-Cu^{2+} exchange interaction responsible for the zero field KD splittings. In order to determine the discrepancies between the experimental splittings and the corresponding Zeeman splittings, each $\langle 1 \rightarrow 2 : D \rangle$-$\langle 2 \rightarrow 1 : D \rangle$ experimental splitting of the GSKD $\rightarrow {}^4I_{15/2}$ spectral range is presented, as well as the corresponding Zeeman calculations, in Fig. 7. Such splittings correspond to the sum of the GSKD and the excited KD splittings. We recall that the discrepancies between the experimental results and the Zeeman calculations are associated with the Nd^{3+}-Cu^{2+} exchange interaction.

Contrary to the $\mathbf{H} \| [001]$ configuration, for which the discrepancies between the experimental results and the Zeeman

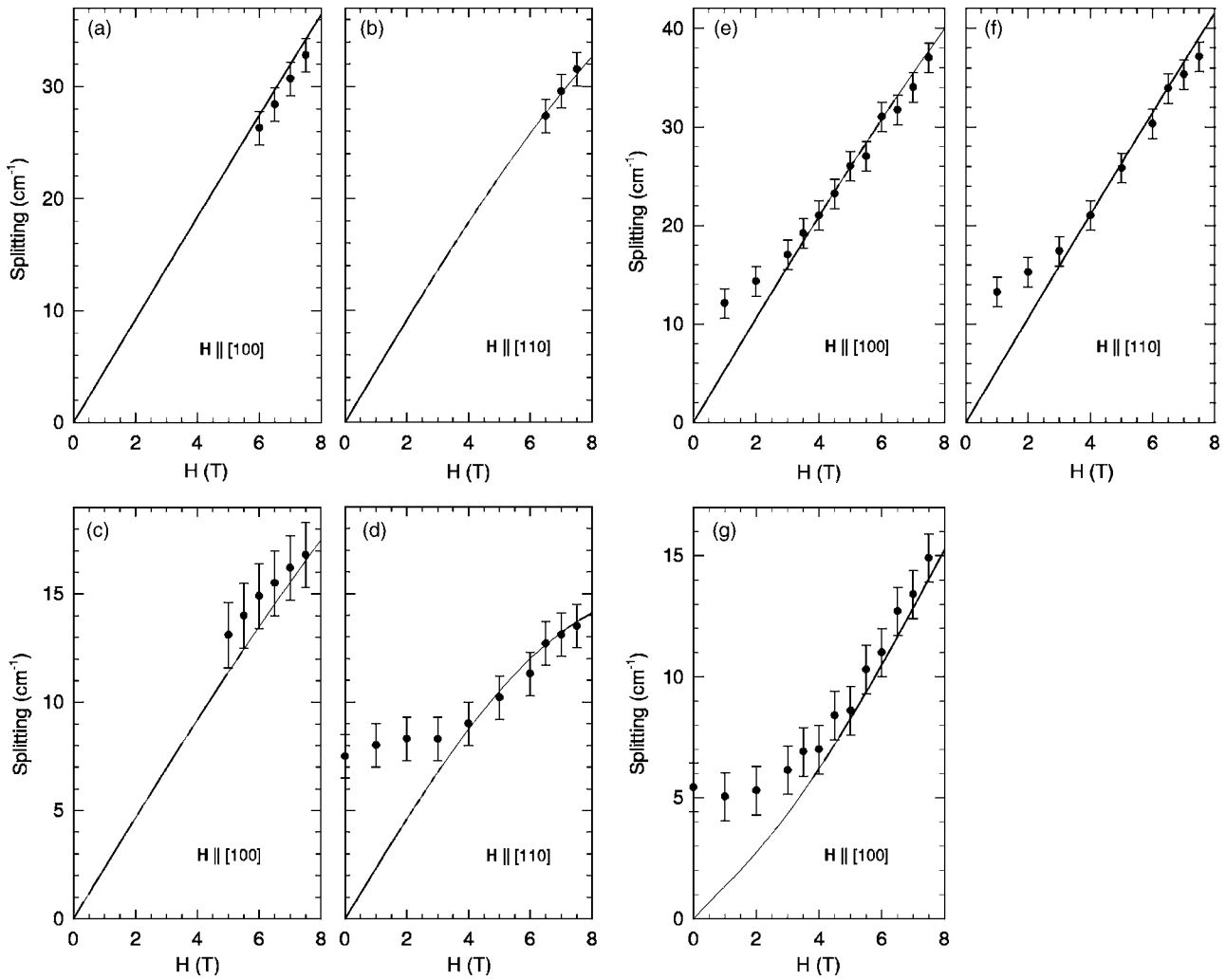

FIG. 7. Experimental splittings (circles) measured in the $^4I_{9/2} \rightarrow {}^4I_{15/2}$ spectral range compared with the Zeeman calculations (lines) obtained for in-plane magnetic fields. The measured splittings correspond to the sum of the ground state doublet splitting and excited doublet splittings, as obtained from the subtraction of the transition wave numbers. (a) and (b), *s-p*; (c) and (d), *v-t*; (e) and (f), *y-x*; (g), *F-D*.

calculations are not significantly modified under a magnetic field of 7.5 T, these discrepancies vanish under a magnetic field larger than $\mathbf{H}_p = 4$ T applied perpendicularly to [001]. Hence, the Zeeman calculations above that critical field fit very well, within the experimental error, the *s-p* [Figs. 7(a) and 7(b)], *v-t* [Figs. 7(c) and 7(d)], *y-x* [Figs. 7(e) and 7(f)] and *F-D* [Fig. 7(g)] experimental KD splittings. This confirms the reliability of the CF parameters given in Table I.[19] Furthermore, these results show that the Nd^{3+} spins align along the applied magnetic field in the collinear phase, rather than perpendicularly. Hence, the Nd^{3+} moments remain perpendicular to their nearest Cu^{2+} neighbors. While Figs. 8(a) and 8(b) illustrate the in-field collinear phase magnetic configuration of Nd_2CuO_4 assuming an intraplane *antiferromagnetic* alignment of the Nd^{3+} spins, for $\mathbf{H} \| [100]$ and $\mathbf{H} \| [110]$, respectively, Figures 8(c) and 8(d) give the corresponding magnetic structure, for $\mathbf{H} \| [100]$ and $\mathbf{H} \| [110]$, respectively, assuming an in-plane *ferromagnetic* alignment of the Nd^{3+} moments.

It is worth mentioning at this point that the relative orientation of the Nd^{3+} and Cu^{2+} magnetic moments within the three-layer-spin units, formed by one Cu^{2+} layer sandwiched between two Nd^{3+} layers, remains the same as the magnetic structure changes from a noncollinear configuration to a collinear one with the in-plane Nd^{3+} spins aligned *antiferromagnetically*. In that case, the intraunit Nd^{3+}-Cu^{2+} anisotropic exchange interaction should not be affected by the noncollinear $\rightarrow$ collinear transitions. This interaction is the most important and is assumed to be mainly responsible for the Nd^{3+} KD splittings. As estimated from the variation of the Nd^{3+} splittings resulting from the Phase II $\rightarrow$ Phase III around 30 K,[16] the interunits interactions are responsible for about 4% only of the whole splittings. Consequently, the Nd^{3+} KD splittings are not expected to be modified significantly by the field-induced magnetic transitions from a noncollinear magnetic configuration to a collinear one. This is in agreement with our results indicating the independence of $\mathbf{H}_p$ on the direction of the magnetic field in the (001) plane.

The Zeeman limit of the Nd^{3+} KD splittings above $\mathbf{H}_p$ implies that the Nd^{3+} magnetic moments are only marginally influenced by the Nd^{3+}-Cu^{2+} anisotropic exchange interaction. This finding is consistent with the magnetization data at $T = 4.4$ K exhibiting paramagnetic behavior.[25] Hence, the

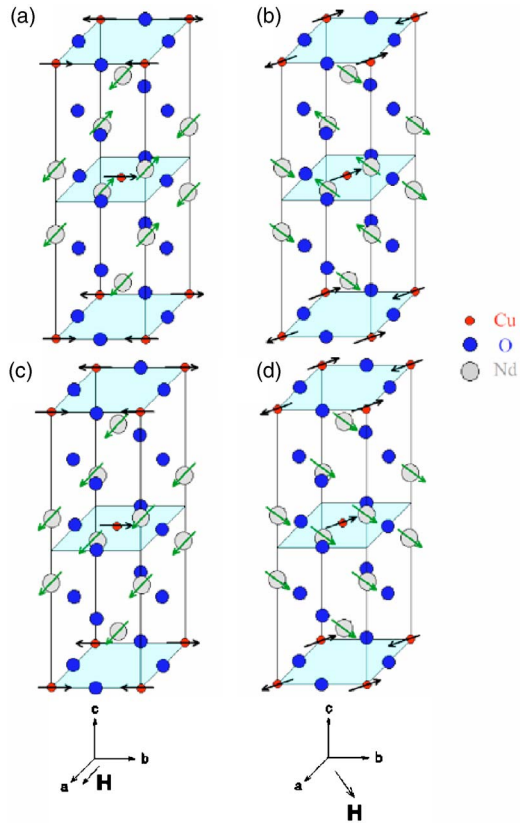

FIG. 8. (Color online) Magnetic configuration of Nd_2CuO_4 in the collinear phase assuming either an antiferromagnetic alignment [(a) $\mathbf{H}\|[100]$; (b) $\mathbf{H}\|[110]$] or a ferromagnetic alignment [(c) $\mathbf{H}\|[100]$; (d) $\mathbf{H}\|[110]$] of the Nd^{3+} spins.

high field magnetic configurations of Nd_2CuO_4 for $\mathbf{H}\|[100]$ and $\mathbf{H}\|[110]$ are those illustrated in Figs. 8(c) and 8(d), respectively. The magnetic field $\mathbf{H}_p$ is then a measure of the intraunit Nd^{3+}-Cu^{2+} anisotropic exchange interaction strength. This interaction vanishes slowly as the Nd^{3+} alignment changes from *antiferromagnetic* to *paramagnetic*, due to the Zeeman interaction. Hence, the *ferromagnetic* alignment of the Nd^{3+} shown in Figs. 8(c) and 8(d) is not favorable to this interaction. Due to the crystal-field environment, the Nd^{3+} lies preferentially along the CuO_2 planes, even in the absence of any exchange interaction. This is responsible for the anisotropic magnetization.[25] Consequently, a field much higher than $\mathbf{H}_p$=4 T is required to align the Nd^{3+} along [001] and thus perturb the original intraunit magnetic configuration. This explains why the contribution of this interaction to the Nd^{3+} KD splittings is not significantly affected at the fields reached in the present study.

A previous specific heat study of Nd_2CuO_4 under magnetic field supports our experimental results.[26] Hence, the Nd_2CuO_4 specific heat data, which exhibit a Schottky anomaly due to the Nd^{3+} GSKD, are not significantly affected by a magnetic field lower than 4 T applied along [110], indicating that the GSKD splitting is only slightly increased. Above 4 T, the position of the Schottky anomaly increases linearly with the magnetic field, in agreement with our Zeeman calculations. No particular shift of the Schottky anomaly is reported concerning the noncollinear $\rightarrow$collinear magnetic transition around 0.75 T. Moreover, the Schottky anomaly is not modified by a field applied along [001], at least for $\mathbf{H}\leqslant 4$ T.

The paramagnetic behavior of the Nd^{3+} ions above 4 T is also consistent with the small in-plane anisotropy of the KD splittings, as shown in Fig. 7. Hence, the predicted *s*-*p* splitting at 7.5 T ($\sim$ 34 cm^{-1}) is around 3 cm^{-1} larger for $\mathbf{H}\|[100]$ [Fig. 7(a)] as compared to $\mathbf{H}\|[110]$ [Fig. 7(b)]. The corresponding experimental anisotropy has been found to be around 1 cm^{-1}. Similarly, the predicted *v*-*t* splitting at 7.5 T ($\sim$ 17 cm^{-1}) is also around 3 cm^{-1} larger for $\mathbf{H}\|[100]$ [Fig. 7(c)] as compared to $\mathbf{H}\|[110]$ [Fig. 7(d)], in agreement with the 3 cm^{-1} anisotropy found experimentally. Finally, the calculated *y*-*x* splitting at 7.5 T ($\sim$ 38 cm^{-1}) is only around 1 cm^{-1} smaller for $\mathbf{H}\|[100]$ [Fig. 7(e)] as compared to $\mathbf{H}\|[110]$ [Fig. 7(f)], in agreement, according to the uncertainties, with the 0 cm^{-1} anisotropy found experimentally.

The KD splittings obtained at 1.6 K as compared with the 8.5 K data indicate that the Nd^{3+}-Nd^{3+} interactions contribute only marginally to the zero field KD splittings. Even though these interactions become important at low temperature due to the large increase of the Nd^{3+} magnetic moments below 10 K,[7] the Nd^{3+} KD splittings decrease only slightly as temperature is decreased from 8.5 to 1.6 K. Moreover, this decrease is an indication that the Nd^{3+}-Nd^{3+} interaction is opposite to both the intraunit Nd^{3+}-Cu^{2+} anisotropic exchange and the Zeeman interactions.

VI. CONCLUSION

In this study, we have shown that while the Nd^{3+} Kramers doublet splittings under a magnetic field applied along [001] cannot be fitted by Zeeman calculations, the splittings are well reproduced by calculations for a magnetic field larger than $\mathbf{H}_p$=4 T applied perpendicularly to [001], irrespective of the in-plane magnetic field orientation and of the noncollinear$\rightarrow$collinear magnetic transitions. Below $\mathbf{H}_p$, the discrepancies between the calculations and the experimental results have been attributed to the Nd^{3+}-Cu^{2+} anisotropic exchange interaction. This interaction vanishes above $\mathbf{H}_p$, which is a measure of the Nd^{3+}-Cu^{2+} anisotropic exchange interaction strength, due to the reorientation transition in the Nd^{3+} subsystem from *antiferromagnetic* to *paramagnetic* state. We have found that the Nd^{3+}-Nd^{3+} interaction is much weaker than the Nd^{3+}-Cu^{2+} anisotropic exchange interaction and opposite to both the Zeeman and the Nd^{3+}-Cu^{2+} anisotropic exchange interaction.

ACKNOWLEDGMENTS

The authors thank J. Rousseau for technical assistance. We also acknowledge support from the National Science and Engineering Research Council of Canada (NSERC) and le Fonds Québécois de la Recherche sur la Nature et les Technologies du Gouvernement du Québec. Also gratefully acknowledged is the Grant Agency of the Czech Republic for its Grant No. 202/03/0552. The work in Prague was also supported by the Institutional Project No. AV0Z1-010-914.

*Electronic address: pierre.richard@bc.edu

[1] H. J. Kang, P. Dai, J. W. Lynn, M. Matsuura, J. R. Thompson, S.-C. Zhang, D. N. Arrgyriou, Y. Onose, and Y. Tokura, Nature (London) **423**, 522 (2003).
[2] T. Uefuji, K. Kurahashi, M. Fujita, M. Matsuda, and K. Yamada, Physica C **378–381**, 273 (2002).
[3] S. Uchida, H. Takagi, and Y. Tokura, Physica C **162–164**, 1677 (1989).
[4] G. M. Luke *et al.*, Phys. Rev. B **42**, 7981 (1990).
[5] M. Matsuda, K. Yamada, K. Kakurai, H. Kadowaki, T. R. Thurston, Y. Endoh, Y. Hidaka, R. J. Birgeneau, M. A. Kastner, P. M. Gehring, A. H. Moudden, and G. Shirane, Phys. Rev. B **42**, 10098 (1990).
[6] J. W. Lynn, I. W. Sumarlin, S. Skanthakumar, W.-H. Li, R. N. Shelton, J. L. Peng, Z. Fisk, and S.-W. Cheong, Phys. Rev. B **41**, R2569 (1990).
[7] P. Richard, M. Poirier, and S. Jandl, Phys. Rev. B **71**, 144425 (2005).
[8] S. Skanthakumar, J. W. Lynn, J. L. Peng, and Z. Y. Li, Phys. Rev. B **47**, R6173 (1993).
[9] Y. Endoh, M. Matsuda, K. Yamada, K. Kakurai, Y. Hidaka, G. Shirane, and R. J. Birgeneau, Phys. Rev. B **40**, 7023 (1989).
[10] A. S. Cherny, E. N. Khats'ko, G. Chouteau, J. M. Louis, A. A. Stepanov, P. Wyder, S. N. Barilo, and D. I. Zhigunov, Phys. Rev. B **45**, R12600 (1992).
[11] S. Skanthakumar, J. W. Lynn, J. L. Peng, and Z. Y. Li , J. Appl. Phys. **73**, 6326 (1993).
[12] R. Sachidanandam, T. Yildirim, A. B. Harris, A. Aharony, and O. Entin-Wohlman, Phys. Rev. B **56**, 260 (1997).
[13] R. Jin, Y. Onose, Y. Tokura, D. Mandrus, P. Dai, and B. C. Sales, Phys. Rev. Lett. **91**, 146601 (2003).
[14] J. P. Hill, A. Vigliante, D. Gibbs, J. L. Peng, and R. L. Greene, Phys. Rev. B **52**, 6575 (1995).
[15] P. Dufour, S. Jandl, C. Thomsen, M. Cardona, B. M. Wanklyn, and C. Changkang, Phys. Rev. B **51**, 1053 (1995).
[16] S. Jandl, P. Richard, V. Nekvasil, D. I. Zhigunov, S. N. Barilo, and S. V. Shiryaev, Physica C **314**, 189 (1999).
[17] A. A. Nugroho, V. Nekvasil, I. Veltruský, S. Jandl, P. Richard, A. A. Menovsky, F. R. de Boer, and J. J. M. Franse, J. Magn. Magn. Mater. **226**, 973 (2001).
[18] T. Strach, T. Ruf, M. Cardona, S. Jandl, V. Nekvasil, C. Chen, B. M. Wanklyn, D. I. Zhigunov, S. N. Barilo, and S. V. Shiryaev, Phys. Rev. B **56**, 5578 (1997).
[19] S. Jandl, P. Dufour, P. Richard, V. Nekvasil, D. I. Zhigunov, S. N. Barilo, and S. V. Shiryaev, J. Lumin. **78**, 197 (1998).
[20] S. N. Barilo and D. N. Zhigunov, Supercond., Phys. Chem. Technol. **2**, 138 (1989).
[21] B. R. Judd, *Operator Techniques in Atomic Spectroscopy* (McGraw-Hill, Inc., New York, 1963).
[22] G. F. Koster, J. O. Dimmock, R. G. Wheeler, and H. Statz, *Properties of the thirty-two point groups* (M.I.T. Press, Cambridge, MA, 1963).
[23] P. Richard, G. Riou, I. Hetel, S. Jandl, M. Poirier, and P. Fournier, Phys. Rev. B **70**, 064513 (2004).
[24] M. F. Hundley, J. D. Thompson, S.-W. Cheong, Z. Fisk, and B. Oseroff, Physica C **158**, 102 (1989).
[25] Y. U. Muzichka, E. A. Goremychkin, I. V. Sashin, M. Diviš, V. Nekvasil, M. Nevřiva, and G. Fillion, Solid State Commun. **82**, 461 (1992).
[26] N. T. Hien, V. H. M. Duijn, J. H. P. Colpa, J. J. M. Franse, and A. A. Menovsky, Phys. Rev. B **57**, 5906 (1998).